Journal of Glaciology (2017), **63**(241) 792–802 doi: 10.1017/jog.2017.45
© The Author(s) 2017. This is an Open Access article, distributed under the terms of the Creative Commons Attribution licence (http://creativecommons.org/licenses/by/4.0/), which permits unrestricted re-use, distribution, and reproduction in any medium, provided the original work is properly cited.

Using an ultra-long-range terrestrial laser scanner to monitor the net mass balance of Urumqi Glacier No. 1, eastern Tien Shan, China, at the monthly scale

CHUNHAI XU,[1,2]* ZHONGQIN LI,[1]* FEITENG WANG,[1] HUILIN LI,[1] WENBIN WANG,[1] LIN WANG[1]

[1]*State Key Laboratory of Cryospheric Sciences/Tien Shan Glaciological Station, Northwest Institute of Eco-Environment and Resources, Chinese Academy of Sciences (CAS), Lanzhou 730000, China*
[2]*University of Chinese Academy of Sciences, Beijing 100049, China*
**Correspondence: Chunhai Xu and Zhongqin Li <xuchunhai716@163.com> and <lizq@lzb.ac.cn>*

ABSTRACT. We describe the use of a terrestrial laser scanner (TLS) to monitor the net mass balance of Urumqi Glacier No. 1, eastern Tien Shan. We used an ultra-long-range Riegl VZ®-6000 TLS, which is specially designed for surveying snow- and ice-covered terrain, to create repeated high spatiotemporal resolution DEMs, focusing on the monthly-scale (25 April–28 May 2015) net mass balance. According to the TLS-derived DEMs, the area of Urumqi Glacier No. 1 was 1.558 km^2 on 25 April 2015 and the average surface elevation change was 0.225 m. By comparing the results from the use of TLS with the conventional glaciological mass-balance method, the correlation coefficient (R^2) between glaciological elevation changes of individual stakes and the TLS-derived geodetic elevation change of corresponding points was 0.85. Considering the uncertainty of both methods, this is a promising result. Using the in situ measured snow densities (snow pits) of the glacier surface, the geodetic net mass balance was 0.074 m w.e., which is slightly positive. The mean uncertainty in the TLS-derived monthly net mass balance was 0.018 m w.e., showing that the TLS surveying system presented accurate and relevant results and is therefore suitable to monitor mass-balance evolution of mountain glaciers.

KEYWORDS: glacier area, glacier surface elevation changes, monthly scale, net mass balance, Riegl VZ®-6000 terrestrial laser scanner

1. INTRODUCTION

Glacier mass balance is a key component of glacier monitoring, which is important for assessing climatic changes, water resources and sea level (IPCC, 2013; Zemp and others, 2015; Slod and others, 2016). Mass balance has been monitored around the world during the last six decades (WGMS, 2013). Traditional glaciological methods provide in situ observations of annual and sometimes seasonal mass balance (Zemp and others, 2013). Ablation can be derived from stake measurements, and snow pits provide accumulation (Cogley and others, 2011). Using the contour-line or profile method, point observations can be extrapolated to glacier-wide mass balance (Østrem and Brugman, 1991; Xie and Liu, 1991; Kaser and others, 2003). The principles of the glaciological observation method are widely accepted. These approaches require dense spatial coverage of in situ observation, which can only be obtained through a succession of intensive measurements of field networks of stakes and snow pits. However, the densities of stake and snow pit observation vary from glacier to glacier and over time (Fountain and Vecchia, 1999; Miller and Pelto, 1999; Van Beusekom and others, 2010), and, because of this and the remote location and dispersed distribution of mountain glaciers (Shangguan and others, 2009) and the inaccessibility of glacier surface areas due to hazardous zones (prone to crevasses, rockfalls or avalanches) (Mehta and others, 2014), most glaciological mass-balance data series consist of just a few years. For the period 1946–2005, 226 glaciers worldwide have mass-balance results, with an average of 15 observation years and 39 glaciers have more than 30 years of measurements, most of the reported series being in North America (WGMS, 2008). In China, only Urumqi Glacier No. 1 has a long mass-balance data series, beginning in 1959 (Li and others, 2007).

Mass balance can be calculated by repeated mapping and differencing of multitemporal DEMs of glacier surface topography using the geodetic observation method and comparing the results with annual in situ measurements using the glaciological method (Zemp and others, 2013). Data sources including theodolite, total station or global navigation satellite systems (Hagen and others, 2005), photogrammetry (Wang and others, 2014), InSAR (Rankl and Braun, 2016) and stereo images (Berthier and others, 2007) mostly restrict the spatial and time resolution of geodetic mass-balance measurements (Thibert and others, 2008; Fischer and others, 2016). In recent years, airborne and terrestrial lidar techniques (e.g. laser scanning) have offered dense point clouds and high-resolution and -precision DEMs of the glacier surface (Joerg and others, 2012; Helfricht and others, 2014; Piermattei and others, 2015). Research shows that the accuracy of geodetic mass balance resulting from the accuracy of the DEMs ranges from 2 m w.e. for photogrammetric data to 0.02 m w.e. for lidar data (Fischer, 2011). Thus, the laborious and time-consuming glaciological method can be supplemented and validated, basal or internal melt processes can be taken into consideration, and extrapolation of point measurements over the entire glacier surface, which is an important source of uncertainty for glaciological mass balance, can be avoided.

https://doi.org/10.1017/jog.2017.45 Published online by Cambridge University Press

Terrestrial laser scanner (TLS) can achieve changes of the mountain cryosphere at very high spatial and temporal resolution (Ravanel and others, 2014). We have used an ultra-long-range TLS (Riegl VZ®-6000) to monitor the net mass balance of Urumqi Glacier No. 1 at the monthly scale. This scanner can acquire high-quality surface elevation information on snow and ice cover over a large range (Gabbud and others, 2015). Most current geodetic mass-balance research focuses on annual or multi-annual scales, while monthly scale has received little attention. This paper describes an application of TLS to monitor the monthly net mass balance and compares direct glaciological and geodetic mass balance at corresponding ablation stakes (points).

2. STUDY SITE

Urumqi Glacier No. 1 (43°06′N, 86°49′E) is a valley glacier located in the Chinese central Tien Shan (Fig. 1a) and is the source of the headwaters of the Urumqi River. It is a north-east-facing valley glacier with an area of 1.59 km^2 in 2012, and elevations of the east and west branches ranging from 3743 to 4267 m a.s.l. and from 3845 to 4484 m a.s.l., respectively. The two branches became separated in 1993 because of continued glacier retreat (Li and others, 2010). Urumqi Glacier No. 1 is a summer-accumulation-type glacier (both accumulation and ablation occur during summer), so the mass balance needs to be monitored in summer (melt season). The glacier has been monitored since 1959; it is one of the reference glaciers of the World Glacier Monitoring Service (WGMS) and a representative glacier in central Asia (Li and others, 2007; Zemp and others, 2009).

3. DATA AND METHODS

3.1. Riegl VZ®-6000 terrestrial laser scanner

Based on time-of-flight measurement with echo digitization and online waveform processing (RIEGL Laser Measurement Systems, 2013), the Riegl VZ®-6000 TLS can acquire dense point clouds of the glacier surface by emitting near-infrared laser signals (Fig. 2). The pulse emitted by the laser transmitter reaches the target object, from which it is reflected back to the laser receiver. A referenced point cloud results from the calculation of the two-way travel time of the pulse (t). The longitudinal (θ) and transverse (φ) scanning angles of the instantaneous survey are captured by the TLS internal measurement. The coordinates of the measured object (x, y, z) are presented according to

$$L = \frac{ct}{2} \tag{1}$$

$$\begin{cases} x = L\cos\theta\cos\varphi \\ y = L\cos\theta\sin\varphi \\ z = L\sin\theta \end{cases} \tag{2}$$

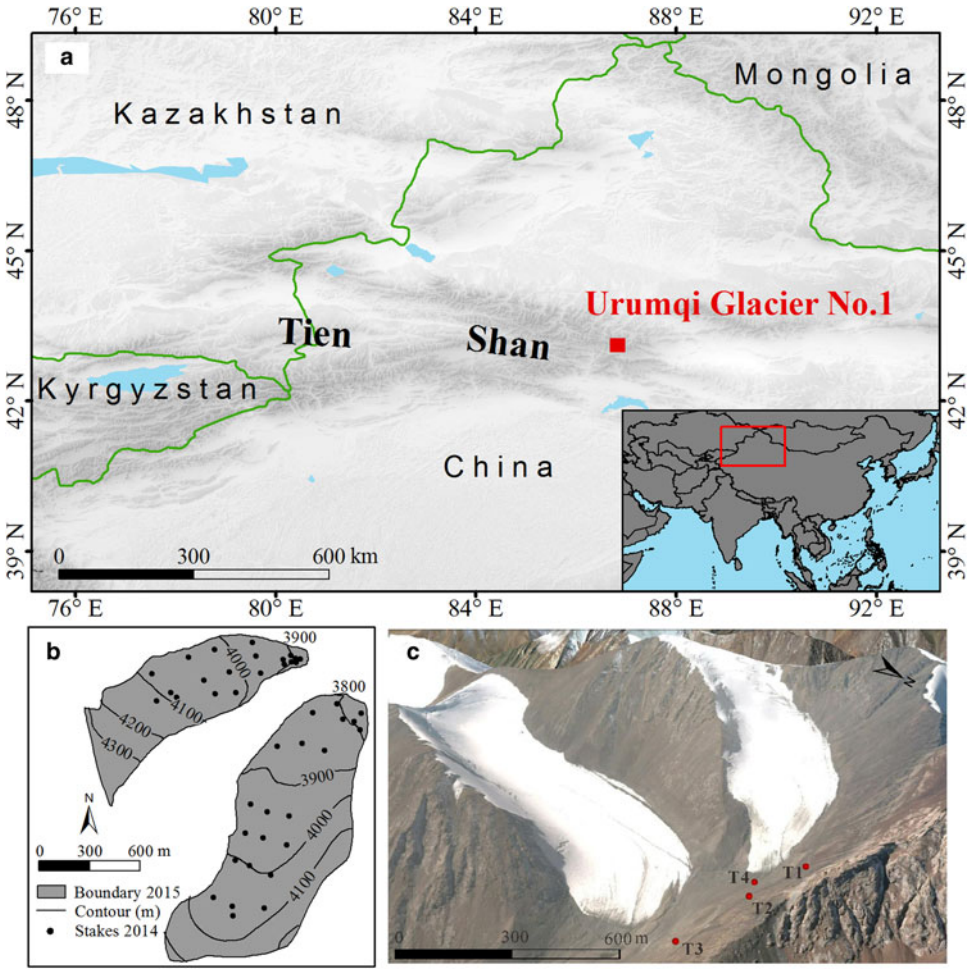

Fig. 1. Study site. (a) Location of Urumqi Glacier No. 1 in the Chinese Central Tien Shan. (b) Measuring point network in 2014, glacier boundary was added based on Fig. 3. (c) Overview of TLS stations at the glacier terminus (image source: Google Earth).

https://doi.org/10.1017/jog.2017.45 Published online by Cambridge University Press

Fig. 2. TLS survey of Urumqi Glacier No. 1 with the Riegl VZ®-6000 terrestrial laser scanner on 25 April 2015. Lower right corner of the picture was a scanning station, which was fixed using reinforced concrete with a GPS-leveling point.

where L is the distance between the laser pulse transmitter and target object, and c is the propagation speed of the laser pulse (RIEGL Laser Measurement Systems, 2014a).

Traditionally, TLS uses class 1 laser beams (wavelengths ~1500 nm), with low reflectance but high absorption over snow and ice cover, and the scanning distance is limited to a few hundred meters (Deems and others, 2013; Gabbud and others, 2015). Riegl VZ®-6000 uses class 3B laser beams (wavelengths ~1064 nm), so high rates of reflection (80%) from snow- and ice- covered terrain and faster surveys (up to 222 000 measurements s^{-1}) are possible even at long distances (up to 6000 m) with high accuracy and precision (Table 1; RIEGL Laser Measurement Systems, 2014a).

3.2. Point cloud data acquisition

In order to quantify geodetic mass balance in detail, four scanning stations with a reinforced concrete structure were installed at the terminus of the glacier (Fig. 1c). Scanning stations T1 and T4 captured the surface point clouds of the west branch and T2 and T3 those of the east branch. On 25 April and 28 May 2015, Riegl VZ®-6000 measurements of Urumqi Glacier No. 1 were performed with the same survey parameters, nearly coincident with days of direct measurements of mass balance (Table 1). To avoid ground motion and to guarantee data quality, the Riegl VZ®-6000 was always mounted on a tripod placed on stable bedrock (scanning stations) around the glacier for each scan (Figs 1c, 2). Three-dimensional (3-D) coordinates of the four scanning stations were obtained using the real-time kinematic (RTK) GPS (Unistrong E650). The horizontal and vertical accuracies of RTK survey stations were ±1 cm + 1 ppm × D and ±2 cm + 1 ppm × D, respectively, where ppm is parts per million and D is the distance (km) between base station and mobile station. The coordinated system of RTK measurement data is the World Geodetic System 1984 (WGS84) (Wang and others, 2016).

Based on high-accuracy 3-D coordinates of the scanning stations, we can quickly and efficiently realize multi-station scanning point clouds registration (a detailed introduction is provided in Section 3.3). In fieldwork, both the data quality and acquisition time must be considered, so surveying parameters are of crucial importance (Table 1). To avoid range ambiguity and to obtain point clouds of the whole glacier surface, laser pulse repetition rates were set to 50 and 30 kHz for rough and fine scanning, respectively (Table 1). The overlap percentage of each scan was above 30%. Surveying parameters of Urumqi Glacier No. 1 are listed in Table 2.

Table 1. Parameters and values of ultra-long-range Riegl VZ®-6000 terrestrial laser scanner (RIEGL Laser Measurement Systems, 2014a)

System parameters	Parameters and values range			
Laser pulse repetition rate	30 kHz	50 kHz	150 kHz	300 kHz
Effective measurement rate	23 000 meas s^{-1}	37 000 meas s^{-1}	113 000 meas s^{-1}	222 000 meas s^{-1}
Max. measurement range for natural targets				
$-\rho \geq 90\%$	6000 m	6000 m	4200 m	3300 m
$-\rho \geq 20\%$	3600 m	3600 m	2400 m	1800 m
Max. number of targets per pulse	up to 15	up to 15	up to 10	up to 9
Accuracy	15 mm	15 mm	15 mm	15 mm
Precision	10 mm	10 mm	10 mm	10 mm
Minimum range	5 m			
Laser wavelength	1064 nm			
Beam divergence	0.12 mrad			
Laser product classification	Laser Class 3B			

https://doi.org/10.1017/jog.2017.45 Published online by Cambridge University Press

Table 2. Riegl VZ®-6000 TLS surveying parameters of Urumqi Glacier No. 1 at the monthly scale

Date 2015	Scanning range m^2	Number of points	Point density m^{-2}	Angle increment °	Number of scans
25 April	3 204 684	12 740 500	3.98	0.02	4
28 May	3 375 116	16 383 175	4.85	0.02	4

3.3. Point cloud data processing

Point cloud data processing was performed using RiSCAN PRO® v 1.81 software (RIEGL Laser Measurement Systems, 2014b). This includes:

(1) Direct georeferencing. The method uses additional sensors (navigation sensors, total station, etc.) to convert the laser scanner's system (Mukupa and others, 2016). We used RTK surveying points of each scanning station to transform the Scanner's Own Coordinate System (SOCS) into a Global Coordinate System (GLCS). The principle can be described as

$$\overrightarrow{r_g} = \overrightarrow{r_0} + R(k)\overrightarrow{r_s} \tag{3}$$

$$R(k) = \begin{bmatrix} \cos k & \sin k & 0 \\ \sin k & \cos k & 0 \\ 0 & 0 & 1 \end{bmatrix} \tag{4}$$

where $\overrightarrow{r_g}$ is the vector of the target in the GLCS, $\overrightarrow{r_s}$ is the vector of the same target in the SOCS, $\overrightarrow{r_0}$ is the vector of SCOS origin in the GLCS, and k is the azimuth between scanning station and backsight target (Lichti and others, 2005).

(2) Point cloud registration (Mukupa and others, 2016). The position of each scan was fixed after direct georeferencing. However, due to the influence of orientation, the point clouds of the overlapped regions cannot coincide completely. A multi-station adjustment was performed based on the iterative closest point (ICP) algorithm (Besl and McKay, 1992; Zhang, 1992). The orientation of each scan was iteratively modified to calculate the best fit between the point patches based on least-squares minimization of residuals (Besl and McKay, 1992; Gabbud and others, 2015).

(3) Point cloud vacuation and filtering. An octree algorithm was applied to the registered scans to generate points with equal spacing to realize point cloud data reduction (vacuation) (Schnabel and Klein, 2006; Perroy and others, 2010), and a terrain filter was used to remove noise and non-ground points (RIEGL Laser Measurement Systems, 2014b).

3.4. Geodetic mass-balance method

In the ArcGIS10.2 software support, interpolation of the processed point generates regular grids (DEMs), and subtraction of the two DEMs provides glacier surface elevation changes. The geodetic observation method determines volume changes by comparing glacier surface elevations of different time periods (Zemp and others, 2013):

$$\Delta V = \sum_{i=1}^{N} \Delta h_i r_i^2 \tag{5}$$

where N is the number of pixels covering the glacier at the maximum extent, $\triangle h_i$ is the elevation difference of the two grids at pixel i, and r_i is the pixel size at pixel i.

To estimate glacier mass balance (B_{geo}), geodetic volume change must be converted to specific mass balance (m w.e.) using

$$B_{geo} = \frac{\Delta V}{S}\frac{\rho}{\rho_{water}} \tag{6}$$

$$S = \frac{S_{t0} + S_{t1}}{2} \tag{7}$$

where ρ is the average density of volume changes, and S is the average glacier area of the two geodetic times, $t0$ and $t1$, assuming a linear change (Thibert and others, 2008; Zemp and others, 2013), which can be considered unchanged at the monthly scale.

3.5. In situ measurements

The mass-balance observation of Urumqi Glacier No. 1 has been implemented using measured points (ablation stakes and snow pits) (Han and others, 2005; Xie and Liu, 2010; Wang and others, 2014). More than 40 ablation stakes were drilled into the glacier surface evenly at different elevations of the east and west branches using a steam drill (Fig. 1b). The hydrological year (mass-balance year) of Urumqi Glacier No. 1 is defined from the previous September 1 to the next August 31 (Liu and others, 1997). The glacier is a summer-accumulation-type glacier; summer runs from the beginning of May to early September each year. A spatial distribution of single-point measurements of ablation and accumulation (snow depth and density) was determined by stakes and snow pits at intervals of a month during the summer. The measurements include the stake vertical height above the glacier surface, superimposed ice thickness and the density and thickness of each snow/firn layer at individual stakes. Stake and snow pit heights were converted into mass (w.e.) to calculate single point mass balance (the summation of snow/firn, superimposed ice and glacier ice mass balance) using measured densities of snow and ice (Xie and Liu, 2010). For Urumqi Glacier No. 1, point mass balance can be extrapolated to glacier-wide mass balance using contour-line and isoline methods (Xie and Liu, 1991).

According to fieldwork in April and May, a larger amount of fresh snow covered the whole glacier surface at the time of TLS measurements (Fig. 2), so we primarily thought about snow/firn mass balance in geodetic method. In order to calculate geodetic mass balance precisely, more than 40 snow pits were dug in the glacier surface to measure the snow density, which were performed on the same days as the TLS survey (Fig. 7a). Interpolation of the snow pits produced

https://doi.org/10.1017/jog.2017.45 Published online by Cambridge University Press

a distributed snow density of the glacier surface, which was set as an average density of the volume changes (Eqn (6)).

3.6. Uncertainty assessment

Uncertainties in the TLS-derived geodetic mass balance include systematic or random errors (Zemp and others, 2013), which can be attributed to: (1) point cloud data acquisition errors, including terrain and atmospheric environment (wind and moisture); (2) data processing errors and DEM creation, i.e. registration (multi-station adjustment), point cloud filtering and interpolation of the raster DEM (smoothing terrain information) (Gabbud and others, 2015; Hartzell and others, 2015; Fischer and others, 2016); and (3) spatial bias of the two DEMs and sampling density of snow and ice (Nuth and kääb, 2011; Zemp and others, 2013).

Point clouds of the glacier were captured in sunny, windless weather, so wind- and moisture-induced errors can be minimized. The octree algorithm built the topological relationship of scattered points to reduce the point cloud, in order to preserve terrain information as much as possible. To eliminate spatial bias of the two DEMs, scanning point clouds of April were set as the reference; a relative registration selects the ground control points of the stable terrain to match the point clouds of the two periods.

The uncertainties of the average TLS-derived glacier surface elevation changes for individual glaciers were quantified based on geostatistical analysis methods (Rolstad and others, 2009), and can be approximated by

$$\sigma^2_{\overline{\Delta h\mathrm{TLS}}} = \sigma^2_{\Delta h\mathrm{TLS}} \times \frac{S_{\mathrm{cor}}}{5S} \tag{8}$$

where S is the glacierized area of the subtracted DEMs, which is really the same as the S defined by Eqn (7) at the monthly scale, S_{cor} is the area over which there are spatial correction errors in the subtraction of the two DEMs, and we conservatively estimate $S_{\mathrm{cor}} = S$ (Fischer and others, 2016). $\sigma_{\Delta h\mathrm{TLS}}$ is the standard deviation for TLS-derived bedrock (stable terrain) elevation changes.

According to Huss and others (2009), the uncertainty σ_{BTLS} in the homogenized mass-balance results from errors in the geodetic mass change:

$$\sigma_{\mathrm{BTLS}} = \pm\sqrt{\left(\overline{\Delta h\mathrm{TLS}} \times \sigma_\rho\right)^2 + \left(\rho \times \sigma_{\overline{\Delta h\mathrm{TLS}}}\right)^2} \tag{9}$$

where σ_ρ is the uncertainty of density. $\overline{\Delta h\mathrm{TLS}}$ is the mean of TLS-derived geodetic elevation changes and the related uncertainty depends on the accuracy of the two DEMs. Resulting values are listed in Table 2 and illustrated in Section 4.3.

4. RESULTS

4.1. TLS-derived glacier area and surface elevation changes

Based on the TLS-derived high-resolution DEM and previous field surveys, we extracted the glacier boundary on 25 April 2015. As shown in Fig. 3, the area of Urumqi Glacier No. 1 was 1.558 km^2, 1.018 km^2 for the east branch and 0.540 km^2 for the west branch. Compared with the latest surveys (GPS-RTK) in 2012 (Wang and others, 2016), the total area decreased by 0.03 km^2, at a rate of 0.01 km^2 a^{-1}.

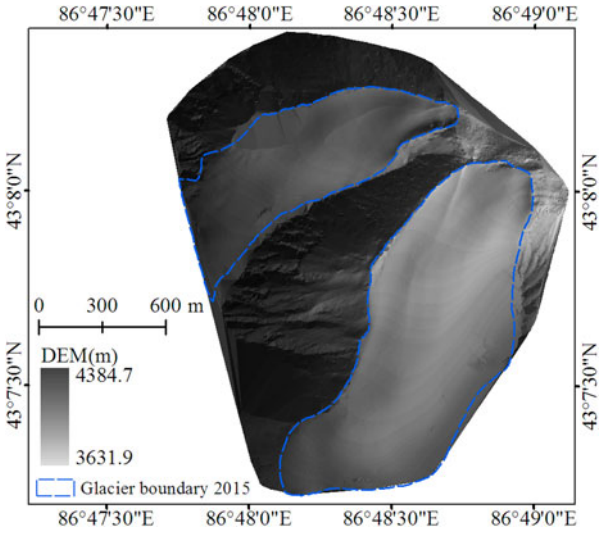

Fig. 3. Extraction of 2015 glacier boundary based on TLS-derived high-resolution DEM and previous field surveying.

As mentioned in Section 4.3, glacier area was an important input parameter for geodetic mass-balance calculation, due to the monthly scale of measurements, so we maintained an unchanged glacier area of 1.558 km^2 as the inputting area parameter.

Surface elevation changes were slightly positive during the study period. Average elevation changes were 0.019 and 0.611 m for the east and west branches, respectively. The mean elevation change was 0.225 m for the total glacier surface; with a glacier volume change of 3.45×10^4 m^3, the mean glacier surface elevation change was 0.007 m d^{-1}. The west branch was more positive than the east branch, mainly because there was more accumulation in the accumulation area of the glacier, which may be related to terrain and altitude factors. The firn basin terrain is steeper in the west branch than the east branch, and the middle–lower part of the west branch has a flat terrain (Fig. 1b), giving rise to mass accumulation and consequent avalanches. An obvious accumulation area can be identified in the west branch (region in blue in Fig. 4), which may have been caused by an avalanche in the upper part (region in light red in Fig. 4). Reduced glacier surface elevation is mainly concentrated in the ablation area of the west branch and the right edge of the east branch, both of which have steeper topographies, which may be adverse to mass accumulation. So the glacial/topographical features of the two branches have important impacts on their dynamics (Xu and others, 2011). It should be mentioned that fresh snow covered the whole glacier surface during the two field measurements. According to field observations, the TLS system captures the surface of snow- and ice-covered terrain (high reflection), and the penetration effect of snow can be ignored. The surface changes therefore included ice and snow.

4.2. Comparison with in situ measurements

Based on the location of individual ablation stakes (Fig. 4), TLS-derived geodetic elevation changes of the stakes were extracted, and were found to match closely the direct glaciological elevation changes (stake height) from in situ measurements, except for a few stakes in the ablation area (Fig. 5). The surface elevation change trends coincided for both methods (Fig. 6), and the correlation coefficient (R^2) for

https://doi.org/10.1017/jog.2017.45 Published online by Cambridge University Press

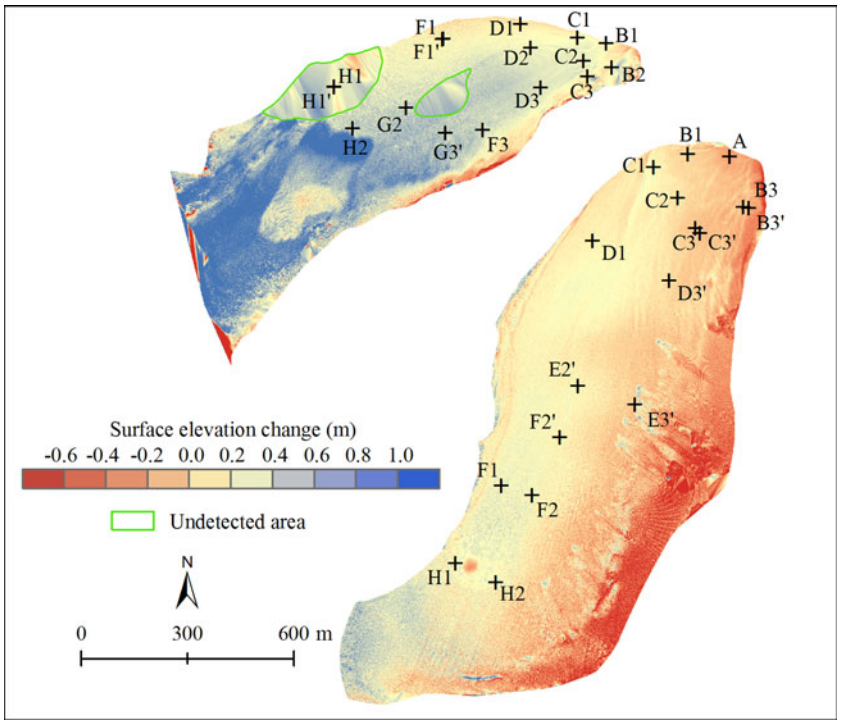

Fig. 4. Spatial distribution of TLS-derived monthly surface elevation changes for Urumqi Glacier No. 1 between 25 April and 28 May 2015. Black crosses show the location of ablation stakes and snow pits. Two green frames indicate areas that cloud not be detected by TLS.

glaciological elevation change of the individual stakes and the TLS-derived geodetic elevation change of corresponding points was 0.85 (passing the 0.001 significance level test). Considering the uncertainties of the two measuring methods and the influence of the terrain factors, differences in surface elevation changes of the point measurements were negligible, indicating that the TLS-derived glacier surface elevation changes were valid. It should be stressed that dynamic thickening and thinning were minor for the monthly scale measurements here.

4.3. TLS-derived glacier monthly net mass balance

To convert glacier volume (elevation) changes to mass balance, the distributed snow density of the total glacier was generated by interpolating in situ measured densities, and then the distributed mass balance was calculated using Eqns (5)–(7) (Fig. 7a). To assess the uncertainty of TLS-derived mass balance, more than 150 stable points in the surrounding bedrock area were selected, and the mean elevation changes and standard deviation of the selected points were −0.011 m and 0.116 m, respectively. Using Eqns (8) and (9), the net mass-balance uncertainty (σ_{BTLS}) was ± 0.018 m w.e., and the TLS-derived mass balance was 0.074 ± 0.018 m w.e., which was slightly positive in the investigated period (Table 3). Based on the two field TLS surveys, plenty of fresh snow covered the whole glacier surface (Fig. 2); the slight accumulation was probably caused by fresh snow cover, which was illustrated in detail in Section 5.2.

Net mass balance versus altitude is important basic information in the Glacier Mass Balance Bulletin reports (WGMS, 2013); Fig. 8 shows the net balance versus altitude of Urumqi Glacier No. 1, with histograms and polylines representing glacier area and net balance in the different altitude regions, respectively. Unlike annual mass balance, the

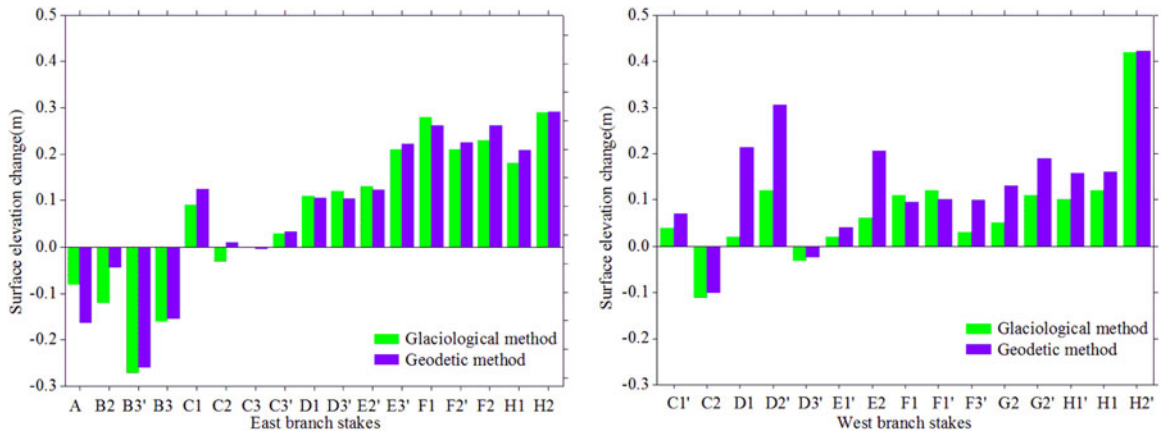

Fig. 5. Comparison between glaciological and geodetic glacier surface elevation changes; the letters represent ablation stakes (Fig. 4).

https://doi.org/10.1017/jog.2017.45 Published online by Cambridge University Press

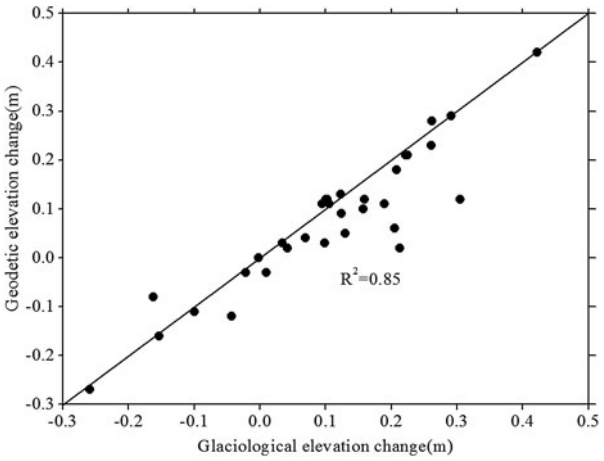

Fig. 6. Relation between glaciological elevation change and geodetic elevation change.

graded law of net mass balance versus altitude was not obvious in the TLS measurements; elevations of the east and west branches were under 3800 and 4000 m a.s.l., where the net mass balance increased with rising altitude. For the east branch, however, the altitude above 3800 m a.s.l. exhibited an opposite trend, potentially caused by ablation on the right side of the back wall region (Fig. 4). The west branch showed a trend relatively well above 4000 m a.s.l.

5. DISCUSSION

5.1. Surveying precautions and point cloud data quality

Generally, the environment (terrain and atmosphere) around the glacierized area is complicated and the quality of TLS survey data is influenced by the surroundings. This paper has shown that an ultra-long-range TLS is well suited for surveying snow- and ice-covered terrain, as it provides precise detail of glacier surface elevation changes. The maximum survey distance of Riegl VZ®-6000 TLS is 6000 m, the total scanning time for the measurement on 25 April was ~46 min and for the measurement on 28 May was ~57 min. The quality of those data and acquisition time depended mainly on the following two matters:

(1) Visual angles of the scanning stations. All the scanning stations should have a field of view wide enough to cover the glacier surface. However, two minimal artifacts existed in the central part of west branch. Although four scans were set at the terminus of Urumqi Glacier No. 1, the artifacts were due to the flatness of the terrain and relatively high altitude of west branch surface (Fig. 1b). Here, the null value regions were filled using spatial interpolation method. Fortunately, we had two stakes (H1 and H1′) in these regions (Fig. 4) and the comparison of the interpolated and measured results was convincing (Fig. 5), indicating the filled portions were reliable. So the artifacts were taken into account to calculate the volume and mass balance.

(2) Atmospheric conditions. Rain, cloud and fog would absorb laser pulse and reduce the possible survey distance; wind might influence the accuracy of point cloud. However, all of those conditions are common around the glacier, so a good weather condition (dry and windless atmosphere) is pre-requisite for TLS survey and data acquisition (Fig. 2). The point cloud data quality can be guaranteed by considering all of these matters.

5.2. Glacier behavior and monthly net mass balance

As Urumqi Glacier No. 1 is located in inner Asia, precipitation and temperature of glacierized areas are the main factors controlling glacier mass balance (Li and others, 2003). In winter, the westerly circulation is affected by the dynamic action of the Tibetan Plateau, inducing cold high-pressure systems to the south of the Tien Shan, which results in a cold and dry climate, with scarce precipitation. In summer, the Tibetan Plateau becomes a thermal depression and shapes a plateau monsoon, which pulls in warm and moist air from India, which in turn produces abundant precipitation around the Plateau. The above-mentioned precipitation and temperature conditions determine Urumqi

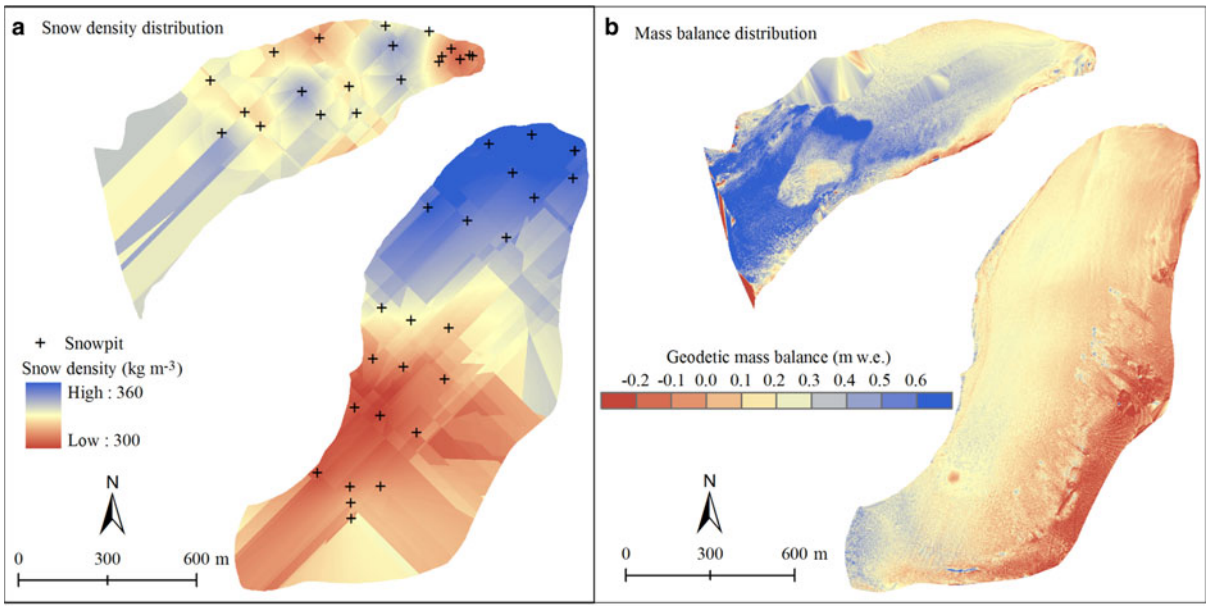

Fig. 7. Distributed snow densities and mass balance for the total glacier from 25 April to 28 May 2015.

https://doi.org/10.1017/jog.2017.45 Published online by Cambridge University Press

Table 3. The average density (ρ) and its uncertainty (σ_ρ), TLS-derived glacier surface elevation changes (ΔhTLS), standard deviation of surface elevation changes ($\sigma_{\Delta h\text{TLS}}$) in stable bedrock area, and uncertainty of mass balance (σ_{BTLS})

Period	ρ kg m^{-3}	σ_ρ kg m^{-3}	ΔhTLS m	$\sigma_{\Delta h\text{TLS}}$ m	σ_{BTLS} m	B_{TLS} m w.e.
25 Apr–28 May 2015	328	31	0.225	0.116	±0.018	0.074 ± 0.018

Glacier No. 1 as a summer-accumulation-type glacier. Namely, the glacier is dominated by weak accumulation from October to next March (winter); the accumulation rate from April to May is faster than in winter; strong ablation and accumulation occur simultaneously during the period June–September (Liu and others, 1997).

It was possible that the slightly positive mass balance observed from the geodetic method was attributable to the assumption of fresh snow cover. According to daily data of Daxigou Meteorological Station (3539 m a.s.l.), at ~3 km south-east of Urumqi Glacier No. 1, the total precipitation was 138 mm and daily mean temperature was −0.3°C during the month (25 April–28 May 2015) (Fig. 9). Numerous studies have shown that air temperature is the most critical factor in determining the precipitation type (Bocchieri, 1980; Czys and others, 1996). It was determined that 98% of the precipitation type was snowfall when temperature fell below 0° (Upadhyay, 1995). Observations indicated most of the precipitation was snow at the headwater of Urumqi River from May to September (Yang and others, 1992b). The precipitation of the nearest two periods (Fig. 9) all occurred before the two TLS surveys. Besides, mean temperature was below 0°C during the two periods, especially the second period (23–27 May), when the mean temperature was −1.2°C (Fig. 9) and we could conclude that the precipitation type (the total precipitation was 35.4 mm) was mainly solid. Glacier melting is directly related to air temperature, which has been well described by positive degree days (the cumulative positive temperatures in a year) (Li and others, 2011). Figure 9 shows that most of the daily mean temperatures were below freezing for several continuous days and considerable amounts of precipitation fell at sub-freezing temperatures, which eventually caused the ablation in seasonal snow layer less than fresh snow derived accumulation. Therefore, the assumption was validated by the meteorological conditions and field observations.

5.3. Applicability of Riegl VZ®−6000 TLS to monitor the mass balance of Urumqi Glacier No. 1

Riegl VZ®-6000 TLS, thanks to its high temporal-spatial resolution and ultra-long-range, has been proved successful in monitoring mass balance of very small glaciers in the Swiss Alps (Fischer and others, 2016) and surface melt of Alpine glaciers at the seasonal and hourly scales (Gabbud and others, 2015). Furthermore, TLS can work without contact with the survey objects and in difficult environments, so allowing to measure dangerous or inaccessible regions of the glacier surface. The surface of Urumqi Glacier No. 1 has been changed with the accelerated shrinkage (Li and others, 2011; Wang and others, 2016). The firn basin and glacier tongue terrain of the west branch have become extremely steep; and the upper right edge terrain of the east branch is also precipitous (Fig. 1b). Hence, it is very difficult for us to insert ablation stakes and dig snow pits in those inaccessible regions. However, glacial terrain and insufficient spatial distribution of stakes have significant influence on extrapolating point observations to glacier-wide mass balance (Yang and others, 1992a; Dyurgerov, 2002; Huss and others, 2009; Xie and Liu, 2010). Besides, according to field observations, steep slopes in the tongue of the west branch are prone to ice avalanches in the ablation season, which cannot be quantified well using the glaciological method.

TLS technology makes it possible for us to monitor those inaccessible regions and quantify the mass loss duo to ice avalanche. In this study, the TLS system measured most of the glacier surface area (Fig. 4) and the comparison of results between TLS-derived and conventional glaciological elevation changes of individual stakes at the monthly scale was promising (Figs 5, 6). In situ measured densities were used to convert TLS-derived elevation changes to mass-balance changes, so the quality of the geodetic net mass balance was very good. We recommend the application of

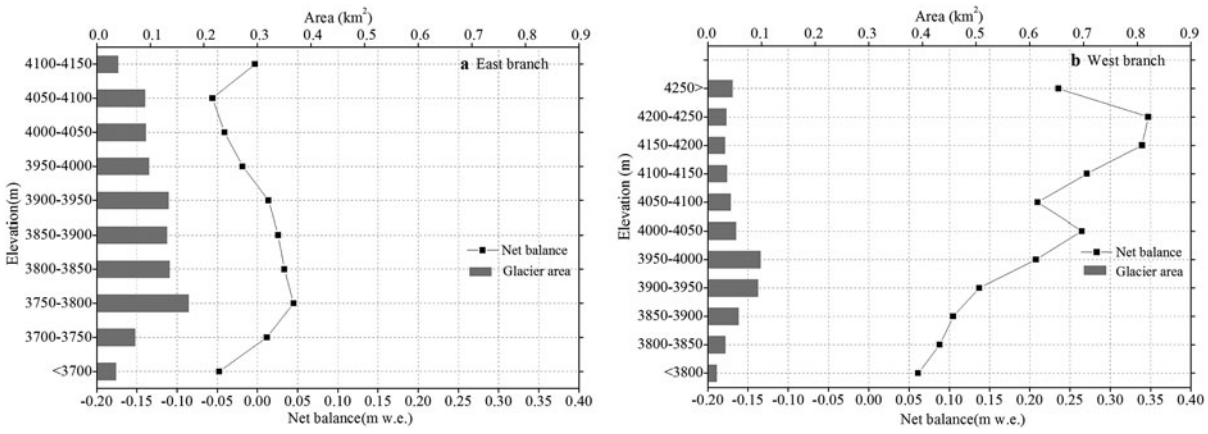

Fig. 8. Monthly net mass balance versus altitude of Urumqi Glacier No. 1.

https://doi.org/10.1017/jog.2017.45 Published online by Cambridge University Press

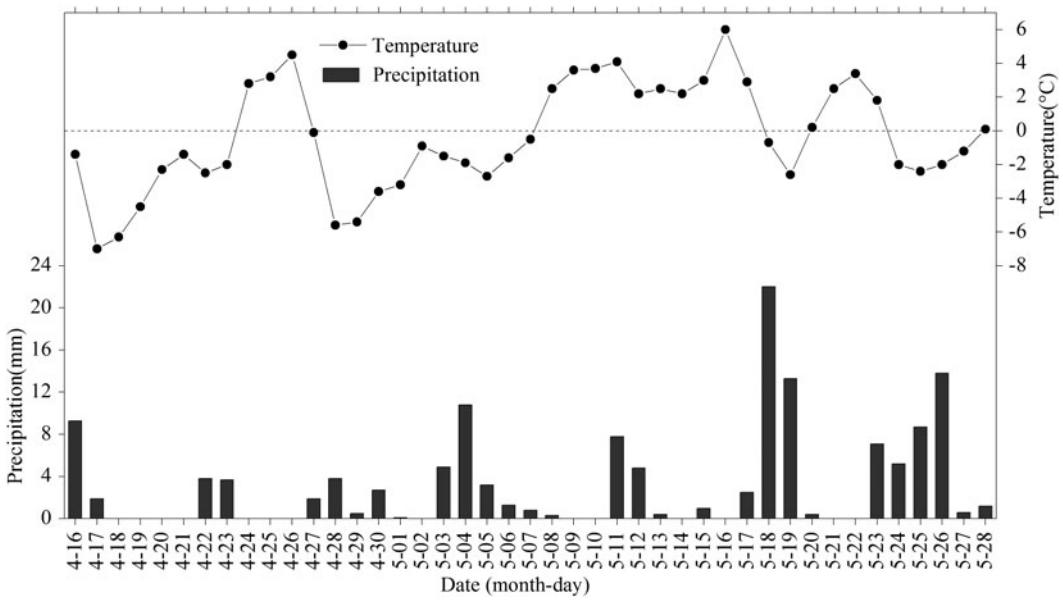

Fig. 9. Daily precipitation and mean temperature observed at the Daxigou Meteorological Station from 16 April to 28 May 2015.

Riegl VZ®-6000 TLS for future mass balance monitoring of Urumqi Glacier No. 1, which will become a beneficial complement to glaciological measurements. From our current experience, although the point cloud data quality can be guaranteed when we follow the field surveying precautions given in Section 5.1, a number of recommendations need to be followed to improve the results: (1) Riegl VZ®-6000 TLS measurements should coincide closely with, and ideally on the same day as, glaciological measurements; (2) fixed scanning stations are necessary between surveys, which could minimize registration errors among the scans of the same time (e.g. on 25 April 2015) and provide better precision of glacier surface elevation changes. In this study each scanning station was fixed using reinforced concrete with a GPS-leveling point (lower right of Fig. 3); (3) the overlap percentage of each scanning station of the same period should be no <30% to achieve a perfect mosaic of multi-station adjustment; (4) plentiful and visible areas of stable bedrock terrain surrounding the whole glacier are needed to guarantee a good quality of the relative registration of different temporal point clouds; and (5) the density of the glacier surface needs to be measured in fieldwork.

At present, the average density of the glacier surface is still a fundamental issue for TLS-derived geodetic mass balance, especially when large amounts of fresh snow cover the glacier surface. Density assumptions of temperate and polythermal glaciers have been researched deeply (Huss, 2013), but little attention has been given to this assumption by Chinese scholars. Most glaciers are cold and multi-thermal glaciers in northwest China (Xie and Liu, 2010), so a density assumption or model based on in situ measured densities is of importance in the next step. We should note that not all glaciers in China have such detailed observations as Urumqi Glacier No. 1, and TLS surveys are ideally carried out at the end of the ablation season to reduce the influence of fresh snow. In addition, the required level of specific knowledge, skills and experience with TLS data acquisition and processing are likely higher than for the conventional glaciological method. It is necessary for us to standardize the processes of TLS measurements and point cloud processing.

6. CONCLUSION

The Riegl VZ®-6000 is specially designed for surveying snow- and ice-covered terrain, and has a ranging accuracy up to 10 mm. The TLS system can monitor surface elevation changes and the mass of mountain glaciers at high spatiotemporal resolution, so the quality of the geodetic net mass balance derived by terrestrial laser scanning is relatively good. We have presented the application of an ultra-long-range TLS to monitor monthly net mass balance. Based on the collection of field data, point cloud data processing and the principle of geodetic mass-balance calculation, we derived surface elevation changes and the geodetic mass balance of Urumqi Glacier No. 1 from 25 April to 28 May 2015.

The TLS-derived high spatial resolution DEM extracted an area of Urumqi Glacier No. 1 of 1.588 km^2 on 25 April 2015. The surface elevation change was 0.225 m, and the correlation coefficient (R^2) between the glaciological elevation change of individual stakes and the TLS-derived geodetic elevation change of corresponding points was 0.85. Using the in situ measured snow density of the glacier surface, the converted geodetic mass balance was 0.074 m w.e., and slightly positive mass balance was due to recent snowfalls.

Mean uncertainty in the TLS-derived monthly net mass balance was 0.018 m w.e. (Table 3). The uncertainty is attributed to data acquisition errors, data-processing and DEM creation errors, the spatial bias of the two DEMs and the sampling density of snow and ice. The next step will be standardizing the processes of TLS measurements and point cloud processing. A density assumption is also significant for TLS-derived geodetic glacier mass balance in northwest China. Despite some uncertainties, the TLS surveying system provided accurate results and is therefore suitable for repeated net mass-balance measurement of mountain glaciers, which can become a beneficial complement to conventional glaciological mass balance.

ACKNOWLEDGEMENTS

We thank the Tien Shan Glaciological Station for field data collection. This research was supported by the National

https://doi.org/10.1017/jog.2017.45 Published online by Cambridge University Press

Natural Science Foundation of China (No. 41471958; No. 91425303; No. 41421061), the Key Research Program of Frontier Sciences of Chinese Academy of Sciences (No. QYZDB-SSW-SYS024) and the West Light Program for Talent Cultivation of Chinese Academy of Sciences. We also thank the two reviewers and Graham Cogley (chief editor) for their careful and constructive comments in improving the manuscript.

REFERENCES

Berthier E and 5 others (2007) Remote sensing estimates of glacier mass balances in the Himachal Pradesh (Western Himalaya, India). *Remote Sens. Environ.*, **108**(3), 327–338 (doi: 10.1016/j.rse.2006.11.017)

Besl P and McKay N (1992) A method for registration of 3-D shapes. *IEEE Trans. Pattern Analysis Machine Intelligence*, **14**(2), 239–256

Bocchieri JR (1980) The objective use of upper air soundings to specify precipitation type. *Mon. Wea. Rev.*, **108**(5), 596–603

Cogley JG and 10 others (2011) *Glossary of glacier mass balance and related terms*. IHP-VII Technical Documents in Hydrology No. 86, IACS Contribution No. 2. UNESCO-International Hydrological Programme, Paris

Czys RR, Scott RW, Tang KC, Przybylinski RW and Sabones ME (1996) A physically based, nondimensional parameter for discriminating between locations of freezing rain and ice pellets. *Wea. Forecasting.*, **11**, 591–598

Deems JS, Painter TH and Finnegan DC (2013) Lidar measurement of snow depth: a review. *J. Glaciol.*, **59**(215), 467–479 (doi: 10.3189/2013JoG12J154)

Dyurgerov M (2002) *Glacier mass balance and regime: data of measurements and analysis*. University of Colorado, Institute of Arctic and Alpine Research, Boulder, CO (INSTAAR Occasional Paper 55.)

Fischer A (2011) Comparison of direct and geodetic mass balances on a multi-annual time scale. *Cryosphere*, **5**(1), 107–124 (doi: 10.5194/tc-5-107-2011)

Fischer M, Huss M, Kummert M and Hoelzle M (2016) Application and validation of long-range terrestrial laser scanning to monitor the mass balance of very small glaciers in the Swiss Alps. *Cryosphere*, **10**(3), 1279–1295 (doi: 10.5194/tc-10-1279-2016)

Fountain AG and Vecchia A (1999) How many stakes are required to measure mass balance of a glacier? *Geogr. Ann. A.*, **81**(4), 563–573 (doi: 10.1111/1468-0459.00084)

Gabbud C, Micheletti N and Lane SN (2015) Lidar measurement of surface melt for a temperate Alpine glacier at the seasonal and hourly scales. *J. Glaciol.*, **61**(299), 963–974 (doi: 10.3189/2015JoG14J226)

Hagen JO, Eiken T, Kohler J and Melvold K (2005) Geometry changes on Svalbard glacier: mass-balance or dynamic response? *Ann. Glaciol.*, **42**(1), 255–261 (doi: 10.3189/172756405781812763)

Han T, Liu S, Ding Y and Jiao K (2005) A characteristics mass balance of glacier No. 1 at the headwaters of the Urumqi River, Tianshan Mountains. *Adv. Earth Sci.*, **20**(3), 298–303 [in Chinese]

Hartzell PJ, Gadomski PJ, Glennie CL, Finnegan DC and Deems JS (2015) Rigorous error propagation for terrestrial laser scanning with application to snow volume uncertainty. *J. Glaciol.*, **61**(230), 1147–1158 (doi: 10.3189/2015JoG15J031)

Helfricht K, Kuhn M, Keuschnig M and Heilig A (2014) Lidar snow cover studies on glaciers in the Ötztal Alps (Austria): comparison with snow depths calculated from GPR measurements. *Cryosphere*, **8**(1), 41–57 (doi: 10.5194/tc-8-41-2014)

Huss M (2013) Density assumptions for converting geodetic glacier volume change to mass change. *Cryosphere*, **7**(3), 877–887 (doi: 10.5194/tc-7-877-2013)

Huss M, Bauder A and Funk M (2009) Homogenization of long-term mass-balance time series. *Ann. Glaciol.*, **50**(50), 198–206 (doi: 10.3189/172756409787769627)

Intergovernmental Panel on Climate Change (IPCC) (2013) *Climate change 2013: the physical science basis. Contribution of working group I to the fifth assessment report of the intergovernmental panel on climate change*. Cambridge University Press, Cambridge

Joerg P, Morsdorf F and Zemp M (2012) Uncertainty assessment of multi-temporal airborne laser scanning data: a case study at an Alpine glacier. *Remote Sens. Environ.*, **127**, 118–129 (doi: 10.1016/j.rse.2012.08.012)

Kaser G, Fountain AG and Jansson P (2003) *A manual for monitoring the mass balance of mountain glaciers*. IHP-VI Technical Documents in Hydrology 59. UNESCO, Paris

Li Z, Han T, Jing Z, Yang H and Jiao K (2003) A summary of 40-year observed variation facts of climate and Glacier No. 1 at headwaters of Urumqi River, Tianshan, China. *J. Glaciol. Geocryol.*, **25**(2), 117–123 [in Chinese]

Li Z and 6 others (2007) Response of glacier melting to climate change-take Urumqi Glacier No. 1 as an example. *J. Glaciol. Geocryol.*, **29**(3), 333–342 [in Chinese]

Li Z, Wang W, Zhang M, Wang F and Li H (2010) Observed changes in stream flow at the headwater of the Urumqi River, eastern Tianshan, central Asia. *Hydrol. Process.*, **24**(2), 217–224 (doi: 10.1002/hyp.7431)

Li Z, Li H and Chen Y (2011) Mechanisms and simulation of accelerated shrinkage of continental glaciers: a case study of Urumqi Glacier No. 1 in Eastern Tianshan, central Asia. *J. Earth Sci.*, **22**(4), 423–430 (doi: 10.1007/s12583-011-0194-5)

Lichti DD, Gordon SJ and Tipdecho T (2005) Error models and propagation in directly georeferenced terrestrial laser scanner networks. *J. Surv. Eng.*, **131**(4), 135–142 (doi: 10.1061/(ASCE)0733-9453(2005)131:4(135))

Liu C, Xie Z and Wang C (1997) A research on the mass balance process of Glacier No. 1 at the headwaters of the Urumqi River, Tianshan Mountains. *J. Glaciol. Geocryol.*, **19**(1), 17–24 [in Chinese]

Mehta M and 5 others (2014) Monitoring of glacier changes and response time in Chorabari Glacier, central Himalaya, Garhwal, India. *Curr Sci.*, **107**(2), 281–289 (doi: 10.13140/2.1.4435.0083)

Miller MM and Pelto MS (1999) Mass balance measurements on the Lemon Creek Glacier, Juneau Icefield, Alaska 1953–1998. *Geoghr. Ann. A*, **81**(4), 671–681

Mukupa W, Roberts GW, Hancock CM and Almanasir K (2016). A review of the use of terrestrial laser scanning application for change detection and deformation monitoring of structures. *Surv. Rev.*, 1–18 (doi: 10.1080/00396265.2015.1133039)

Nuth C and Kääb A (2011) Co-registration and bias corrections of satellite elevation data sets for quantifying glacier thickness change. *Cryosphere*, **5**(1), 271–290 (doi: 10.5194/tc-5-271-2011)

Østrem G and Brugman M (1991) *Glacier mass balance measurements: a manual for field and office work*. Environment Canada, National Hydrology Research Institute (NHRI Science Report 4.), Saskatoon, SK.

Perroy RL, Bookhagen B, Asner GP and Chadwick OA (2010) Comparison of gully erosion estimates using airborne and ground-based LiDAR on Santa Cruz Island, *California*. *Geomorphology*, **118**(3), 288–300 (doi: 10.1016/j.geomorph.2010.01.009)

Piermattei L, Carturan L and Guarnieri A (2015) Use of terrestrial photogrammetry based on structure-from-motion for mass balance estimation of a small glacier in the Italian Alps. *Earth Surf. Process. Land.*, **40**(13), 1791–1802 (doi: 10.1002/esp.3756)

Rankl M and Braun M (2016) Glacier elevation and mass changes over the central Karakoram region estimated from TanDEM-X and SRTM/X-SAR digital elevation models, *Ann. Glaciol.*, **51**(71), 273–281 (doi: 10.3189/2016AoG71A024)

https://doi.org/10.1017/jog.2017.45 Published online by Cambridge University Press

Ravanel L, Bodin X and Deline P (2014) Using Terrestrial Laser Scanning for the recognition and promotion of High-Alpine geomorphosites. *Geoheritage*, **6**(2), 129–140 (doi: 10.1007/s12371-014-0104-1)

RIEGL Laser Measurement Systems (2013) *Preliminary data sheet, 07.05.2013; riegl VZ-6000 – 3D ultra long range terrestrial laser scanner with online waveform processing*. RIEGL Laser Measurement Systems, Horn, Austria

RIEGL Laser Measurement Systems (2014a) *3D terrestrial laser scanner Riegl VZ®-4000/Riegl VZ®-6000 general description and data interfaces*. RIEGL Laser Measurement Systems, Horn, Austria

RIEGL Laser Measurement Systems (2014b) RiSCAN PRO® – Version 1.8.1. Riegl Laser Measurement Systems, Horn, Austria

Rolstad C, Haug T and Denby B (2009) Spatially integrated geodetic glacier mass balance and its uncertainty based on geostatistical analysis: application to the western Svartisen ice cap, Norway. *J. Glaciol.*, **55**(192), 666–680 (doi: 10.3189/002214309789470950)

Schnabel R and Klein R (2006) Octree-based point-cloud compression. In Proceedings of Eurographics Symposium on Point Based Graphics, Boston, MA, USA, 111–120 (doi: 10.2312/SPBG/SPBG06/111-120)

Shangguan D and 5 others (2009) Glacier changes during the last forty years in the Tarim Interior River basin, northwest China. *Progr. Natur. Sci.*, **19**(6), 727–732 (doi: 10.1016/j.pnsc. 2008.11.002)

Sold L and 8 others (2016) Mass balance re-analysis of Findelengletscher, Switzerland; benefits of extensive snow accumulation measurements. *Front. Earth Sci.*, **4**(18) (doi: 10.3389/feart.2016.00018)

Thibert E, Blanc R, Vincent C and Lane SN (2008) Instruments and methods glaciological and volumetric mass-balance measurements: error analysis over 51 years for Glacier de Sarennes, French Alps. *J. Glaciol.*, **54**(186), 522–532 (doi: 10.3189/002214308785837093)

Upadhyay DS (1995) *Cold climate hydrometeorology*. John Wiley, New York, NY

Van Beusekom AE, O'Neel SR, March RS, Sass LC and Cox LH (2010) Re-analysis of Alaskan benchmark glacier mass-balance data using the index method. *USGS Scientific Investigations Report* 2010-5247, 16 p

Wang P, Li Z, Li H, Wang W and Yao H (2014) Comparison of glaciological and geodetic mass balance at Urumqi Glacier No. 1, Tian Shan, central Asia. *Global Planet. Change.*, **114**, 14–22 (doi: 10.1016/j.gloplacha.2014.01.001)

Wang P and 7 others (2016) Analyses of recent observations of Urumqi Glacier No. 1, Chinese Tianshan Mountains. *Environ. Earth Sci.* **75**(8), 1–11 (doi: 10.1007/s12665-016-5551-3)

WGMS (2013) *Glacier mass balance bulletin No. 12 (2010–2011)*. ICSU(WDS)/IUGG(IACS)/UNEP/ UNESCO/WMO, World Glacier Monitoring Service, Zürich (doi: 10.5904/wgms-fog-2013-11)

World Glacier Monitoring Service (WGMS) (2008) *Global glacier changes: facts and figures*. UNEP, World Glacier Monitoring Service, Zürich. http://www.grid.unep.ch/glaciers/

Xie Z and Liu C (1991) Measurement method and main characteristics of the glacier mass balance in Asia. In Kovar K and Nachtnabel HP, ed. *Application of geographic information systems in hydrology and water resources*. Proc. HydroGIS 93 Conference, April 1993, Vienna, 453–459. IAHS Publ. no. 211

Xie Z and Liu C (2010) *Introduction to glaciology*. Shanghai Popular Science Press, Shanghai, 1–490 [in Chinese]

Xu X, Pan B, Hu E, Li Y and Liang Y (2011) Response of two branches of Glacier No. 1 to climate change from 1993 to 2005, tianshan, China. *Quat. Int.*, **236**(1–2), 143–150 (doi: 10.1016/j.quaint.2010.06.013)

Yang D, Liu C, Wang C, Elder K and Kattelmann R (1992a) Studies of measurement and calculation methods of accumulation on Glacier No. 1. *J. Glaciol. Geocryol.*, **14**(1), 1–10 [in Chinese]

Yang D, Kang E and Blumer F (1992b) Characteristics of precipitation in the source area of the urumqi river basin. *J. Glaciol. Geocryol.*, **14**(3), 258–266 [in Chinese]

Zemp M, Hoelzle M and Haeberli W (2009) Six decades of glacier mass-balance observations: a review of the worldwide monitoring network. *Ann. Glaciol.*, **50**(50), 101–111 (doi: 10.3189/172756409787769591)

Zemp M and 16 others (2013) Reanalysing glacier mass balance measurement series. *Cryosphere*, **7**(4), 1227–1245 (doi: 10.5194/tc-7-1227-2013)

Zemp M and 38 others (2015) Historically unprecedented global glacier decline in the early 21st century. *J. Glaciol.*, **61**(228), 745–762 (doi: 10.3189/2015JoG15J017)

Zhang Z (1992) Iterative point matching for registration of free-form curves. *Int. J. Comput. Vision*, **13**, 119–152 (doi: 10.1007/BF01427149)

MS received 3 March 2017 and accepted in revised form 14 July 2017; first published online 18 August 2017

https://doi.org/10.1017/jog.2017.45 Published online by Cambridge University Press